TITLE OF SYMPOSIUM, JOURNAL, OR MANUAL: Zirconium in the Nuclear Industry: Thirteenth International Symposium, Annecy, France, June 10-14, 2001, ASTM Special Technical Publication 1423.

AUTHOR'S NAMES:

R. S. Daum[1], S. Majumdar[2], D. W. Bates[3], A. T. Motta[4], D. A. Koss[5], and M. C. Billone[6]

TITLE OF PAPER:

On the Embrittlement of Zircaloy-4 Under RIA-Relevant Conditions*

AUTHORS AFFILIATIONS:

[1]Assistant Engineer, [2]Senior Engineer, and [6]Engineer and Program Manager, Energy Technology Division, Argonne National Laboratory, Argonne, IL 60439-4838.

[3]Graduate Student (Currently, U.S. Navy), [4]Assistant Professor, [5]Professor, The Pennsylvania State University, University Park, PA 16802.

ABSTRACT: The extended use of Zircaloy cladding in light water reactors degrades its mechanical properties by a combination of irradiation embrittlement, coolant-side oxidation, hydrogen pickup, and hydride formation. The hydrides are usually concentrated in the form of a dense layer or rim near the cooler outer surface of the cladding. Utilizing plane-strain ring-stretch tests to approximate the loading path in a reactivity-initiated accident (RIA) transient, we examined the influence of a hydride rim on the fracture behavior of unirradiated Zircaloy-4 cladding at room temperature and 300°C. Failure is sensitive to hydride-rim thickness such that cladding tubes with a hydride-rim thickness >100 μm (≈700 wppm total hydrogen) exhibit brittle behavior, while those with a thickness <90 μm (≈600 wppm) remain ductile. The mechanism of failure is identified as strain-induced crack initiation within the hydride rim and failure within the uncracked ligament due to either a shear instability or damage-induced fracture. We also report some preliminary results of the uniaxial tensile behavior of low-Sn Zircaloy-4 cladding tubes in a cold-worked, stress-relieved condition in the transverse (hoop) direction at strain rates of 0.001/s and 0.2/s and temperatures of 26-400°C.

KEYWORDS: mechanical properties, ring stretch specimens, Zircaloy-4 cladding, hydrides, hydride rim, stress-state, fracture strain

Introduction

During steady-state operation of light water reactors, the mechanical behavior of the zirconium-based fuel cladding degrades due to a combination of oxidation, hydriding, and radiation damage. In an effort to increase operating efficiency through the use of longer fuel cycles, and to reduce the volume of waste associated with core reloads, utilities have a strong incentive to increase the average discharge burnup of the fuel assemblies. Further increases in operating efficiency of power reactors can also be achieved by increasing the coolant outlet temperature. However, both of these changes in reactor operation enhance cladding degradation, which may increase the likelihood of cladding failure during design-basis accidents.

One such postulated design-basis accident scenario is the reactivity-initiated accident (RIA) in a pressurized water reactor (PWR) caused by the ejection of a control rod from the core, which would cause a rapid increase of reactivity and thermal energy in the fuel [*1*]. The increase in fuel temperature resulting from an RIA induces a rapid fuel expansion at strain rates as high as 10/s, causing a severe pellet-cladding mechanical interaction (PCMI). This PCMI forces the cladding into multiaxial tension such that the maximum principal strain is in the hoop (i.e., transverse) direction of the cladding tube. The survivability of cladding irradiated to high fuel burnup under postulated RIA conditions is thus a response to a combination of the mechanics of loading and the material degradation during reactor exposure [*1*]. Recent research has shown that cladding ductility during an RIA may be degraded at high burnup [*1*], and there are ongoing research efforts to address this issue. Three effects are primarily responsible for the loss of ductility of Zircaloy cladding at high burnup: radiation damage, radiation-induced changes in precipitate composition and morphology, and hydriding. Radiation damage from fast neutrons causes a population of dislocation loops to be created, which has a pronounced effect on

hardening during the initial exposure to a fast neutron flux. However, this increase in dislocation loop density is thought to saturate at relatively low exposures (see references cited in [*2*]). Hardening due to changes in precipitates may saturate at higher neutron fluence levels [*3*]. Hydriding, which is the major subject of this study, increases with burnup. The combined effect of these three phenomena is a progressive increase in hardening and a decrease in ductility with in-reactor exposure (e.g., see Refs. [*4,5*]).

The influence of a *uniform* distribution of hydrides on the tensile ductility of zirconium-based alloys has been studied extensively (e.g., see Refs. [*6-12*]). However, when compared to the ductility behavior in these previous laboratory studies, an RIA event involving high burnup fuel presents two important *new* conditions that affect cladding response: (a) non-uniformly distributed hydrides in the form of a layer or rim and (b) failure under a multi-axial tension stress state. The first condition arises because, when cladding picks up hydrogen in the presence of a heat flux, the temperature gradient through the cladding thickness causes hydrides to precipitate preferentially near the cooler outer surface. This precipitation forms a hydride rim, which resides above a substrate that is relatively free of hydrides. Given the texture in the Zircaloy-4 cladding tubes used in light water reactors, the hydride layer consists of aligned, circumferentially oriented hydride platelets [*5, 6*]. A prediction of the ductility of such cladding must take into account the presence of the hydrides as a layer/rim, the ability of the hydrides to deform [*6, 7, 10*], their circumferential orientation within the hydrided layer, and the presence of a relatively unhydrided substrate. It is possible that some dissolution of the hydrides may occur during initial heat-up.

With regard to the second condition, the deformation behavior of high burnup cladding with hydrides is sensitive to the stress state. It is well known that elevating the level of the stress

triaxiality ratio decreases the fracture strain of recrystallized Zircaloy sheet containing uniform distributions of hydrides [*8, 9*]. Conducting a laboratory test to assess the safety of Zr alloy cladding during an RIA presents difficulties. One of these difficulties is that the multi-axial stress state experienced by the cladding during an RIA is not well known and may actually vary as the transient develops. The pellet-cladding interaction during an RIA forces the cladding to deform under a multi-axial tensile stress state, generally regarded to be in the range $1 \leq \sigma_\theta/\sigma_z \leq 2$, where σ_θ is the hoop stress component and σ_z is the axial stress component. More specifically, the thermal expansion mismatch considerations of the PCMI imply a stress state of equal biaxial tension ($\sigma_\theta/\sigma_z = 1$); however, the axial path of cladding cracks in RIA tests [*15,16*] suggests $\sigma_\theta > \sigma_z$ or $\sigma_\theta/\sigma_z > 1$. We believe a stress state relevant to the analysis of cladding behavior during an RIA is that imposed by the transverse, plane-strain, ring-stretch tension test, for which a procedure has been recently developed [*13,14*]. In this case, owing to the plastic anisotropy of the Zircaloy cladding (R = 2.3 for unirradiated Zircaloy-4 tubing, where R = width-strain/thickness-strain in uniaxial hoop tension), a plane-strain deformation path imposes multi-axial tension such that $\sigma_\theta/\sigma_z \cong 1.4$.

The primary purpose of this study is to explore the response of non-irradiated Zircaloy-4 cladding tubes that contain hydrides concentrated in the form of a thin layer near the outer surface, as is typical of high-burnup cladding, when tested under conditions relevant to RIA. Using ring specimen geometries in order to impose uniaxial tension and multi-axial tension in the hoop direction, we have determined the mechanical properties and the direct influence of thin layers of hydrides on the ductility of Zircaloy-4 cladding tubes. We have also examined the cladding failure process to identify and quantify the failure mechanisms that control the observed fracture strains.

In addition to identifying an accurate failure criterion, prediction of cladding behavior during an RIA event depends critically on its deformation behavior and the constitutive laws that describe that behavior. While such data are available for the axial deformation behavior of cladding tubes, relatively little has been reported in the open literature describing the uniaxial tension behavior in the *hoop* direction of Zircaloy-4 cladding. Thus, we also present results describing the uniaxial ring-stretch deformation behavior of low-Sn Zircaloy-4 cladding tubes in a cold-worked, stress-relieved (CWSR) condition that have been tested at strain rates of 0.001/s and 0.2/s and at temperatures from 26-400°C.

The results for the mechanical behavior of unirradiated Zircaloy-4 with and without added hydrogen provide baseline data for future tests to be performed with high burnup cladding samples. As these samples will have radiation damage, radiation-induced changes in precipitate composition and morphology, and outer and inner surface oxidation, as well as hydrides, the data from this future study will help to determine the separate effects of hydrides on the strength, ductility, and failure modes of cladding irradiated to high fuel burnup.

Experimental Procedure

Materials

As in previous studies [*13,14*], Zircaloy-4 cladding tubes were obtained from Sandvik Special Metals and Framatome Cogema Fuels in the CWSR condition with outer diameters of approximately 9.5 and 10.8 mm and wall thicknesses of about 0.56 and 0.69 mm, respectively. The grain structure consists of elongated grains with ≈10:1 aspect ratio, oriented parallel to the tube axis. The elongated grains are ≈10-15 μm long and ≈1-2 μm thick. As reported elsewhere [*13*], the as-fabricated Sandvik Zircaloy-4 possesses a crystallographic texture in which the basal

planes tend to align with their basal poles inclined 25° to 60° to the normal of the tube surface and oriented toward the tangential direction. The prism poles show a strong tendency to align along the tube axis, which is also consistent with previous observations for such cladding. As reported elsewhere, the measured pole figures for this cladding show basal and prism pole intensities above four and up to ten times their random value [*13*].

To simulate the hydrogen distribution in high-burnup cladding, unirradiated cladding tubes were artificially hydrided in an argon/hydrogen gas mixture at 327°C (600 K) by M. Ozawa at Nuclear Development Corporation according to a proprietary process similar to that reported elsewhere [*18*]. Hydride distributions were developed during gas charging such that the hydrides were concentrated within a hydride rim of controlled thickness near the outer surface of the cladding tube, as will be described later. The total oxygen content of hydrogen-charged cladding was found to be approximately equal to that of as-fabricated cladding.

Ring Stretch Testing

The cracking geometry of irradiated fuel cladding, when tested under RIA-type loading, indicates failure by through-thickness slip and under a biaxial state of stress [*1, 15-16*]. However, in the absence of any constraints across the gauge width, uniaxial specimens fail by slip across the gauge width, such that extensive specimen width contraction occurs [*13*], unlike in RIA-type failures. Therefore, we have utilized a specially designed ring-stretch specimen geometry to impose a near plane-strain state of stress such that we can produce cladding deformation with hoop extension followed by a fracture path of through-thickness slip, similar to the hoop deformation that would be expected during an RIA. As described elsewhere [*13,14*], a "transverse plane-strain" specimen with double edge notches, shown in Fig. 1a, was used. The

constraints of the two notches in this specimen force the central region of the gauge section to deform such that little contraction occurs across the specimen width during the test. Because of this configuration, a condition of near plane-strain deformation condition is achieved, as has been supported by finite element modeling and by detailed measurements of the local ratio of thickness to hoop strain.

While the plane-strain ring-stretch test was used to determine failure conditions in the hydrogen-embrittlement part of this study, a uniaxial ring-stretch test specimen and procedure was used to determine the deformation response in the hoop direction of the cladding tube. The uniaxial ring-stretch specimen geometry, shown in Fig. 1b, has a gauge length-to-width ratio of four in conjunction with lubrication between the specimen gauge section and loading grips to promote uniform deformation within the gauge section [*14*]. As in previous studies [*13,14,17*], microhardness indentations were used to determine strains on a local basis, as shown in Fig. 1 for both plane-strain and uniaxial specimens. For both non-hydrided cladding and hydrided cladding with varying hydride rim thickness, it was found that crack or failure initiation rarely coincided with microhardness indentations, and thus, the indentations did not induce surface cracks. This procedure enabled us to determine local plastic strains with an accuracy of ± 0.01. Most of the uniaxial tests were performed at an initial strain rate of $\approx 10^{-3}$/s; limited tests were also performed at a strain rate of ≈0.2/s. The loading fixtures used for the plane-strain ring stretch tests consist of two "D-shaped" die inserts, which transmit the displacement to the specimen. To minimize friction effects and promote uniform deformation along the gauge section, we rely on lubrication using a combination of Teflon™ tape and vacuum grease between the die inserts and the inner surface of the cladding specimen [*13*]. Tests on un-irradiated/un-hydrided specimens confirm relatively uniform deformation along a gauge section somewhat

greater than 2 mm long in the specimen shown in Fig. 1a [*13, 14*]. For the uniaxial specimen testing, which has been described elsewhere [*14,17*], similar "D-shaped" loading fixtures were used along with a well-lubricated (fine film of tungsten disulfide with Teflon™ tape and vacuum grease) central insert to mitigate the effects of bending and friction between loading grips and the specimen gauge section.

Specimens were machined from cladding tubes using a traveling-wire electro-discharge machine (EDM); for hydrided specimens, total hydrogen contents near EDM cuts did not increase and were within experimental error as compared to the as-hydrided cladding. Radiant and resistive furnaces were used to heat specimens at a rate of ≈5°C/s with an error in testing temperature of ±7°C.

Results and Discussion

Microstructure

Figure 2 shows the hydride distributions in irradiated and artificially charged Zircaloy cladding. The resulting microstructures consist of circumferential hydrides concentrated primarily within a layer near the outer surface of the cladding tube, thus forming a "hydride rim." In the case of the artificially charged specimens, the thicknesses of the hydride rim were controlled and ranged from approximately 20 to 250 μm. In both of the cases shown in Fig. 2, a few hydrides exist within the "substrate" layer of the cladding tube below the rim of hydrides. The artificially hydrided specimens tend to have a relatively uniform and high concentration of hydrides within the hydrided rim (see Fig. 2a). Such a dense concentration of hydrides is frequently observed in high-burnup cladding, as shown in Fig. 2b. Occasionally, a few hydrides are also observed near the inner surface of irradiated cladding (see Fig. 2b).

On the Failure Process

In the current study, the presence of the hydride rim results in the initiation of microcracks soon after yielding. Cladding fracture may thus be viewed as a three-stage process: (i) microcrack initiation, (ii) growth and linkage of short cracks within the hydride rim to a long surface crack, and (iii) growth of the long crack through the remaining substrate ligament below the hydride rim. In the first stage, crack initiation in the hydrided rim is observed to occur at very small strains (essentially zero strain). The resulting cracks have a number density that is influenced by the thickness of the hydride layer, such that the density of initiated cracks decreases with increasing hydride layer thickness. Thus, thick hydride layers typically initiate a single, long deep crack, while thin hydride rims initiate a population of many short cracks. The second stage is a closely related two-step process involving the growth and linking of shorter cracks into a long crack *and* the subsequent growth of the long crack. This process results in specimen ductility and appears to depend both on the density of cracks *and* on their depth. Crack initiation through a thick hydride layer (i.e., a deep crack) usually results in a long deep crack spanning the width of the specimen. Such a crack propagates relatively easily through the cladding thickness, resulting in near brittle behavior of the material. However, as the crack depth decreases (i.e., thin hydride layers), the density of the short microcracks increases, and linking of these short cracks into a long crack requires additional plastic strain. In addition, the propagation of these long but shallow cracks through the unhydrided ligament remains difficult. As a result, cladding with thin hydride layers (i.e., 20 to 80 μm thick) forms a population of shallow, short cracks that must link prior to propagating through the cladding thickness. Cladding ductility then results from both the crack linking process and the through-thickness crack growth. However, at hydride layers greater than 100 μm, it becomes easier for

short (but deeper) cracks along the specimen length to form a long deep crack. The presence of such a long deep crack is sufficient to cause near brittle fracture. The process described above causes a gradual ductile-to-brittle transition as the hydride rim thickness increases from 50 to 140 μm.

Following crack initiation and linking/growth to a long crack along the cladding surface, cladding extension and eventual fracture depend on the plasticity/crack-growth characteristics of the uncracked ligament. If hydride concentrations are low within this ligament *and* the temperature is sufficiently high (e.g., 300°C) such that the substrate is quite ductile and resistant to crack growth, cladding fracture will essentially be a result of a deformation localization process within the uncracked ligament. In this case, ductility results as the shear localization develops, resulting in large, local crack opening displacements and the large peak strains in Fig. 4. Thus at 300°C, the fracture surface profile consists of a "normal" fracture through the hydride layer, followed by shear localization along a plane inclined through the thickness at an angle of roughly 45° to the cladding surface. Figure 5a provides support for this fracture sequence for a unirradiated specimen. Importantly, as seen in Fig. 5b, we call attention to the observation that the fracture of Zircaloy cladding irradiated to high-burnup, which contains a hydride layer near the outer surface and was subjected to the loading of a simulated in-reactor RIA transient, has a very similar fracture profile even though failure likely occurred near room temperature. In this case, the very low strain hardening (possibly due in part to dislocation channeling) of the irradiated cladding promotes the shear localization within the cladding beneath the hydride layer.

At room temperature, the reduced ductility of the unhydrided substrate induces an alternative failure mode of the uncracked ligament, as shown in Fig. 5c. In this case, crack initiation through the hydride rim is followed by ductile fracture induced by damage

accumulation involving void nucleation (at fractured hydrides) and void growth. Both void nucleation and growth are quite sensitive to normal stresses, and the resulting fracture surface is the plane of largest normal stress, or the plane *normal* to the maximum principal stress, as shown in Fig. 5c. Consistent with the above hypothesis, Figure 6 shows a scanning electron micrograph of a typical fracture surface of failed hydrided specimens with failure of uncracked ligament occurring via a damage accumulation process. Note the transition in fracture mode from near-brittle fracture within the hydride layer such that brittle fracture of the hydrides is linked by ductile tear ridges within the Zircaloy matrix. In contrast, ductile microvoid formation and coalescence (but also on a plane normal to the tensile axis) occurs in the remaining unhydrided ligament.

In summary, localized necking and shear failure of the uncracked ligament will likely be favored at 300°C, where a decrease in strain hardening and increase in damage-induced fracture strain promotes localization [*13,19,20*]. Given the small value of strain hardening in irradiated Zircaloy [*21*], it is not surprising that high-burnup cladding, such as that shown in Fig. 5b, fails in a manner suggesting that a shear instability governs final material separation after the hydride rim cracks.

On Determining a Fracture Strain

In this study, we define the *fracture* strain (ε_{frac}) to include the sum of the displacements accumulating during crack linking and growth, and we include those crack-opening displacements of cracks that open but do not propagate (i.e., arrest) in the underlying ductile ligament. On the basis of the failure sequence depicted above and in Fig. 4, the strain distribution (shown in Fig. 4b) for a failed hydrided Zircaloy specimen can be used to determine

fracture strain. We recognize that, after cracks initiate within the hydrided rim, Fig. 4b indicates an additional cladding hoop extension, as deformation localization/fracture develops within the uncracked ligament. The local strains vary with position depending on proximity to the crack flanks, at which location the local strain is expected to decrease to the crack initiation strain or nearly zero strain. Thus, we assume contributions to the cladding ductility (ε_{frac}) from those crack-opening displacements of non-propagating cracks.

The ε_{frac}-value can be determined experimentally in the following manner. The specimens had two rows of the hardness indentations that we used as grids to determine hoop strain values at a given location and at intervals of 0.2 mm. The fracture strain is then calculated from the following equation:

$$\varepsilon_{frac} = \frac{\sum_i (\varepsilon_i \cdot \Delta y_i)}{\sum_i \Delta y_i} \qquad (1)$$

where ε_i is the local interval strain, and Δy_i = 0.2 mm. We deliberately chose this numerical summation *not* to include the extension associated with crack-opening displacements of the *fatal* crack that results in specimen fracture. However, the summation assumes continuity of strain, as defined by the strains adjacent to the main crack, and, importantly, it includes contributions to the total cladding extension at fracture from cracks that open but do not propagate.

For high-burnup cladding containing a thin layer of hydrides near the outer surface, observations of the cross sections of cladding fractured during RIA-type tests indicate a fracture process similar to that described above. Importantly, the fracture surface profile shown in Fig. 5b, which is typical of most of the RIA-simulation tests of high-burnup cladding and which is similar to Fig. 5a, can be readily understood on the basis of the failure process. Thus, if local strain data are available, a determination of failure strains using the above procedure should

indicate not only a reasonable failure condition, but also the mechanism by which a hydride rim controls the failure of the cladding during the RIA event. While such a study will also be performed on irradiated *and* hydrided cladding in future testing, we present below results based on unirradiated cladding containing hydride rim layers of varying thicknesses.

Effect of Hydride Layers on Ductility

Figure 7 shows the dependence of the fracture strains on thickness of the hydride rims and total hydrogen content in Zircaloy cladding tubes deformed to failure at near plane-strain tension at room temperature and 300°C (these results are also shown in numerical form in the Appendix). It is important to recognize that these ring-stretch tests impose a biaxial stress state that results in near plane-strain deformation path with the major principal strain component being the hoop strain. The most important trend in Fig. 7 is the obvious dependence of cladding ductility on hydride-rim thickness (see Fig. 7a). At both room temperature and 300°C, there appears to be a gradual ductile-to-brittle transition with increasing hydride layer thickness. Specifically, cladding with hydride rims of thicknesses ≥140 μm show little or no plastic deformation to failure. In view of the fact that the experimental accuracy of our measurements of local strain is ± 0.01, we concluded that these cladding tubes are essentially brittle. At the 100-μm hydride thickness level, there may be a small level of plastic deformation to the cladding prior to failure. However, cladding samples with hydride-rim thicknesses <90 μm are distinctly ductile with hoop failure strains of roughly 0.04 or greater. We have not collected sufficient data to detect the expected influence of temperature on the ductile-to-brittle transition.

As an alternative approach to examining the influence of hydrogen on failure of the Zircaloy, Figure 7b presents the dependence of fracture on total hydrogen content. The brittle

cladding with a thick hydride rim had total hydrogen contents ≥700 wppm. Although most of the ductile specimens had hydrogen contents in the 300-600 wppm range, ductility was also observed in specimens with thin hydride layers in excess of 700 wppm hydrogen. Therefore, comparing Figures 7a and 7b, it is clear that the ductile-to-brittle transition as a function of hydride rim thickness is *sharper* or more definable than the similar transition as a function of total hydrogen content. For example, in Fig. 7b, several results are in the 500-1000 wppm range with similar hydrogen concentrations but widely varying values of ductility. This is because these samples have different hydride layer thicknesses, and thus, thickness is the predominant factor in causing failure.

Comments on Failure of Hydrided Zircaloy

This work and previous studies clearly indicate that hydrides have a strong effect on the ductility of Zircaloy. It is also clear that Zircaloy ductility does not depend solely on the total hydrogen concentration and testing temperature, but also on the hydrogen distribution and the stress state used in the testing. To illustrate the first point, we note that Zircaloy-4 cladding having a *uniform* hydride distribution is brittle above 1000 wppm hydrogen when tested under plane-strain conditions. In contrast, when the hydrides are concentrated in a rim, the material can be brittle at H concentrations as low as 500 wppm (if a 100-μm hydride rim is formed). Thus, the localization of the hydrides onto a hydride rim causes a loss of cladding ductility, as compared to the homogeneously hydrided material. As mentioned above, this condition is caused by the opening of cracks in the hydride layer and the subsequent failure of the subjacent material by either a deformation localization or damage accumulation process.

To illustrate the second point, we refer to the research of Bai and co-workers [*10*], who demonstrated that uniformly hydrided Zircaloy is ductile up to at least 1100 wppm hydrogen and shows only a 50% decrease in ductility at 2000 wppm hydrogen when tested under *uniaxial* tension at 350°C. In contrast, when tested under plane-strain tension, uniformly hydrided Zircaloy cladding at 1000 wppm fails in a brittle manner (<1% ductility) at 300°C. The difference in the two results can be ascribed, in part, to the small difference in test temperature, but more importantly, to the fact that plane-strain tension is a more severe stress state than uniaxial tension, as recognized previously [*9*].

Thus, for uniformly distributed hydrides, the factor controlling the ductile-to-brittle transition is the overall hydrogen level, while for samples with a hydride rim, the thickness of that rim is the predominant factor.

On Transverse Stress-Strain Properties

Uniaxial ring-stretch specimens were machined from as-fabricated cladding (no hydrogen) and tested under thermal and mechanical loadings relevant to the RIA transient in order to obtain baseline stress-strain data for comparison to irradiated cladding. Figure 8 shows results of yield strength (YS) and ultimate tensile strength (UTS) and uniform elongation as a function of temperature and strain rate for the Zircaloy deformed in the *hoop* direction of the cladding tube.

As shown in Fig. 8a, the Zircaloy exhibits strain-rate hardening and strain-rate sensitivity (m), such that $m = d(\ln\sigma)/d(\ln\dot{\varepsilon})$ and is found to depend on temperature, where σ is the true stress, and $\dot{\varepsilon}$ is the strain rate. This study and previous studies have reported a strain-hardening exponent (n) value of 0.06 from compression and tensile tests of specimens oriented for hoop

deformation, where $n = d(\ln\sigma)/d(\ln\varepsilon)$ and ε is the true plastic strain [*13,14*]. For deformation in the axial direction of Zircaloy-4 in the CWSR and unirradiated condition, limited room-temperature testing has found $n = 0.07$ [*13,14*].

Figure 8b shows uniform elongation to be relatively insensitive to temperature and to have a nominal value of 0.06 at low strain rates, which is consistent with the measured *n*-values. There appears to be a small decrease in uniform elongation at the higher strain rate for all testing temperatures.

Summary

We have conducted hoop tension tests to examine the deformation and fracture behavior of unirradiated Zircaloy-4 cladding under microstructural/stress-state conditions relevant to those anticipated in a postulated Reactivity-Initiated Accident (RIA) reactor transient. The microstructural conditions included precipitation of hydrides to form a hydride rim near the outer surface of the cladding. The biaxial stress state used primarily in this study resulted in near plane-strain tension in the hoop direction of the cladding tube. We believe such a multi-axial stress state is relevant to assessing the survivability of Zircaloy cladding during an RIA. We also conducted preliminary transverse uniaxial tests of Zircaloy cladding at various temperatures and strain rates to establish a baseline for later testing of irradiated cladding. The main conclusions are as follows:

1. When tested under plane-strain conditions, cladding ductility in the hoop direction is very sensitive to hydride-rim thickness at both room temperature and 300°C. This sensitivity is manifested in a ductile-to-brittle transition with increasing hydride rim thicknesses, such that

the cladding is ductile when the hydride rim thickness is less than 90 μm, but it is brittle at hydride rim thicknesses of approximately 140 μm.

2. The mechanism of failure of hydrided cladding is identified as strain-induced cracking of the hydrided rim layer and subsequent failure of the uncracked ligament by either damage-induced fracture (room temperature) or by a shear instability (300°C).
3. A comparison of these results with previous studies based on uniform hydride distributions in Zircaloy illustrates that Zircaloy ductility does not depend solely on the total hydrogen concentration, but also on the hydride distribution and the stress state.
4. Preliminary results of the uniaxial tensile behavior of unirradiated, non-hydrided cladding tubes deformed in the *transverse (hoop)* direction at strain rates of 0.001/s and 0.2/s and at temperatures from 26-400°C indicate decreases in yield and tensile strengths with increasing temperature and decreasing strain rates.

Acknowledments

This research was supported by the U.S. Nuclear Regulatory Commission, Office of Nuclear Regulatory Research and under Contract No. W-31-109-ENG-38 with the U.S. Department of Energy. We thank Mr. Ozawa, of NDC in Japan, for his expert preparation of tubing samples with controlled hydride rims. We thank Ross Bradley at Sandvik Special Metals and Bert Dunn at Framatome Cogema Fuel for supplying the Zircaloy samples used in this study. The authors would like to thank T. Bray, H. Tsai, H. Chung, I. Prokofiev, W. Kettman, D. McGann, and D. Pushis of Argonne National Laboratory for technical discussions and experimental assistance.

REFERENCES

[1] Meyer, R. O., McCardell, R. K., Chung, H. M., Diamond, D. J., and Scott, H. H., "A Regulatory Assessment of Test Data for Reactivity Initiated Accidents," *Nuclear Safety*, 37 [4], 1996, pp. 271-288.

[2] Lemaignan, C. and Motta, A. T., "Zirconium in Nuclear Applications," *Nuclear Materials*, 10B, B.R.T. Frost, ed. New York: VCH, 1994, pp. 1-52.

[3] Chung, H. M., Yaggee, F. L., and Kassner, T. F., "Fracture Behavior and Microstructural Characteristics of Irradiated Zircaloy Cladding," Zirconium in the Nuclear Industry: 7th International Symposium, R. B. Adamson and L. F. P. Van Swam, Eds., ASTM STP 939, 1987, pp. 775-80.

[4] Yasuda, T., Nakatsuka, M., and Yamashita, Zirconium in the Nuclear Industry: 7th International Symposium, R. B. Adamson and L. F. P. Van Swam, Eds., ASTM STP 939, 1987, pp. 734-747.

[5] Garde, A. M., Zirconium in the Nuclear Industry: 8th International Symposium, ASTM STP 1023, L. F. P. Van Swam and C. M. Eucken, eds., 1989, pp 548-569.

[6] Coleman, C. E. and Hardie, D., "The Hydrogen Embrittlement of Alpha Zirconium-A Review," *Journal of Less-Common Metals*, 2, 1966, pp. 168-185.

[7] Ells, C. E., "Hydride Precipitates in Zirconium Alloys," *Journal of Nuclear Materials,* 28, 1968, pp. 129-151.

[8] Simpson, L. A., "Criteria for Fracture Initiation at Hydrides in Zirconium-2.5% Niobium Alloy," *Metallurgical Transactions A*, 12A , 1981, pp. 2113-2124.

[9] Fan, Y. and Koss, D. A., "The Influence of Multiaxial States of Stress on the Hydrogen Embrittlement of Zirconium Alloy Sheet," *Metallurgical Transactions A*, 16A , 1985, pp. 675-681.

[10] Bai, J. B., Prioul, C., and Francois, D., "Hydride Embrittlement in Zircaloy-4 Plate: Part I. Influence of Microstructure on the Hydride Embrittlement in Zircaloy-4 at 200°C and 350°C," *Metallurgical and Materials Transactions A*, 25A, 1994, pp. 1185-1197.

[11] Garde, A. M., Smith, G. P., and Pirek, R. C., "Effects of Hydride Precipitate Localization and Neutron Fluence on the Ductility of Irradiated Zircaloy-4," in *11th International Symposium on Zirconium in the Nuclear Industry*, ASTM STP 1295, 1996, pp. 407-430.

[12] Grange, M., Besson, J., and Andrieu, E., "Anisotropic Behavior and Rupture of Hydrided Zircaloy-4 Sheets," *Metallurgical and Materials Transaction A*, 31A, 2000, pp. 679-690.

[13] Link, T. M., Koss, D. A., and Motta, A. T., "Failure of Zircaloy Cladding under Transverse Plane-strain Deformation," *Nuclear Engineering and Design*, 186, 1998, pp. 379-394.

[14] Daum, R. S., Majumdar, S., Tsai, H., Bray, T. S., Koss, D. A., Motta, A. T., and, and Billone, M. C., "Mechanical Property Testing of Irradiated Zircaloy Cladding under Reactor Transient Conditions," *Proceeding of the 4th International Symposium on Small Specimen Test Techniques*, ASTM STP 1418, 2002, in press.

[15] Fuketa, T., Ishijima, K., Mori, Y., Sasajima, H., and Fujishiro, T., "New Results from NSSR Experiments with High Burnup Fuel," *Proceedings of the Twenty-Third Water Reactor Safety Information Meeting*, NUREG/CP-0149, 1995, pp. 45-63.

[16] Ishijima, K. and Fuketa, T., "Progress of the RIA Experiments with High Burnup Fuels and their Evaluation in JAERI," *Proceedings of the Twenty-Fourth Water Reactor Safety Information Meeting*, NUREG/CP-0157, 1996, pp. 93-105.

[17] Bates, D. W., Koss, D. A., Motta, A. T., and Majumdar, S., "Influence of Specimen Design on the Deformation and Fracture of Zircaloy Cladding," *Proceedings of the ANS International Topical Meeting on LWR Fuel Performance*, American Nuclear Society, Park City, Utah, 2000, pp. 1201-1210.

[18] Nagase, F. and Uetsuka, H., "Hydride Morphology and Hydrogen Embrittlement of Zircaloy fuel Cladding used in NSRR/HBO Experiment," *Proceedings of the ANS International Topical Meeting on LWR Fuel Performance*, American Nuclear Society, Portland, OR, 1997, pp. 677-687.

[19] Link, T. M., Koss, D. A., and Motta, A. T., "Strain Localization in Sheet Metal Containing a Geometric Defect," *Metallurgical and Materials Transactions A*, 31A , 2000, pp. 1883-1886.

[20] Z. Marciniak and J. Duncan, *Mechanics of Sheet Metal Forming*, London: E. Arnold, 1992.

[21] SCDAP/RELAP5/MOD2, Code Manual volume 4: MATPRO: "A Library of Materials Properties for Light Water Reactors Accident Analysis," *NUREG/CR-5273, EG-2555, Chapter 4.9*, 1990.

Appendix

TABLE 1 -- Limit Strains and Crack Initiation Strains for Hydrided Zircaloy-4

Specimen No.	Temperature, °C	[H], wppm	Hydride Rim Thickness, μm	Fracture Strain (ε_{frac})
AR#5	26	40	0	0.07
B2#2	26	586	86	0.034
N24#3	26	1050	140	0.01
A1#2	26	762	148	0.005
N24#1	26	1140	181	0
N26#1	26	1776	245	0
NRW#1	300	40	0	0.08
N7W#1	300	300	19	0.048
N7R#1	300	580	42	0.062
A2Y#2	300	825	73	0.058
A2Y#1	300	*	75	0.047
B2#3	300	707	95	0.07
B2#5	300	847	101	0.02
A1#3	300	889	140	0.013
A1#1	300	794	141	0.016
N24#2	300	1043	173	0
N26#2	300	1800	264	0

* Total hydrogen content not determined.

Figure Captions

FIG. 1 – (a) Plane-strain and (b) uniaxial ring-stretch test specimens with micohardness indentation arrays for determining true plastic strains in the hoop direction of the cladding (all dimensions are in millimeters and not-to-scale).

FIG. 2 – Transverse micrographs showing hydride microstructure and distribution of (a) hydrogen-gas-charged, non-irradiated specimen of Zircaloy-4 cladding (N7R#1) with a hydride rim thickness of ≈42 μm (note the arrows delineating hydride rim) and (b) Zircaloy-4 cladding irradiated to 50 GWd/MTU [*15*].

FIG. 3 – Scanning electron micrographs at (a) low magnification (45X) and (b) higher magnification (150X) showing Mode I surface cracking of a plane-strain specimen (A1#2) with a hydride rim of 148 μm that was tested at room temperature.

FIG. 4 – (a) Schematic of Mode I cracks with respect to microhardness indentation array and corresponding schematic of strain distribution of Indent Row #2 (dimensions in millimeters and not-to-scale) and (b) actual strain distribution of plane-strain ring-stretch specimen (N7R#1) with hydride layer thickness of 42 μm tested at 300°C.

FIG. 5 – Transverse fracture profiles of Zircaloy-4 in (a) hydrided, non-irradiated condition (specimen B2#5 with a hydride rim of 101 μm that was tested at 300°C), (b) hydrided, irradiated condition [*15*] showing Mode I cracking of hydride layer followed by shear instability, and (c) hydrided, non-irradiated condition (specimen B2#2 with a hydride rim of 86 μm that was tested at room temperature) showing Mode I cracking of hydride layer followed by ductile microvoid coalescence.

FIG. 6 – Scanning electron micrograph of fracture surface of a hydrided, non-irradiated specimen (N26#1) with a hydride rim of 245 μm that was tested at room temperature. Near-

brittle fracture of hydride layer is followed by ductile microvoid coalescence within the remaining ligament.

FIG. 7 – Fracture strain (ε_{frac}) at room temperature and 300°C as a function of (a) hydride layer thickness and (b) total hydrogen content.

FIG. 8 – (a) Yield and ultimate tensile strengths and (b) uniform elongation for non-irradiated cladding as a function of temperature and strain rate.

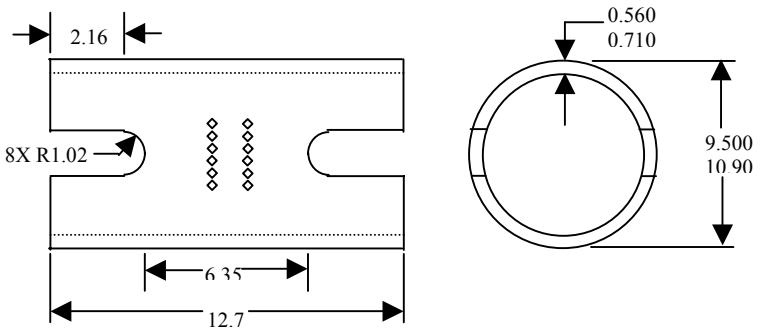

(a)

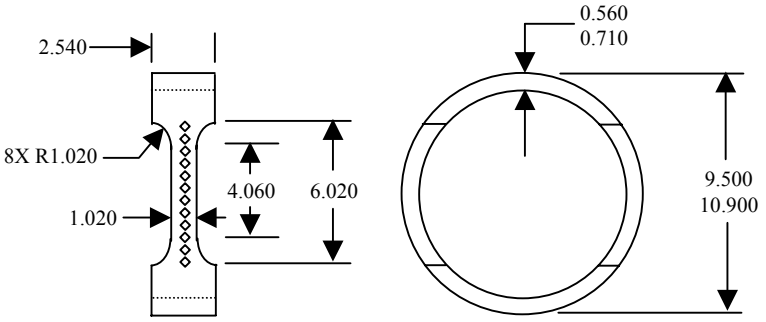

(b)

FIG. 1 – (a) Plane-strain and (b) uniaxial ring-stretch test specimens with micohardness indentation arrays for determining true plastic strains in the hoop direction of the cladding (all dimensions are in millimeters and not-to-scale).

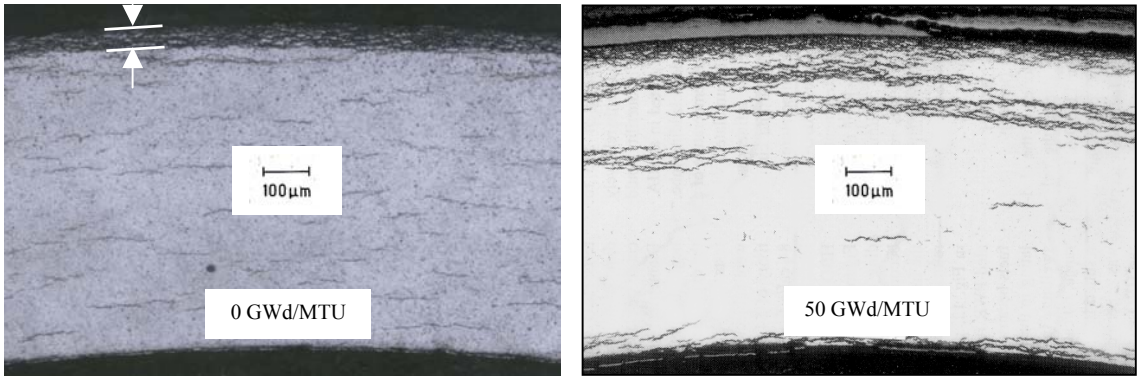

(a) (b)

FIG. 2 – Transverse micrographs showing hydride microstructure and distribution of (a) hydrogen-gas-charged, non-irradiated specimen of Zircaloy-4 cladding (N7R#1) with a hydride rim thickness of ≈42 µm (note the arrows delineating hydride rim) and (b) Zircaloy-4 cladding irradiated to 50 GWd/MTU [*15*].

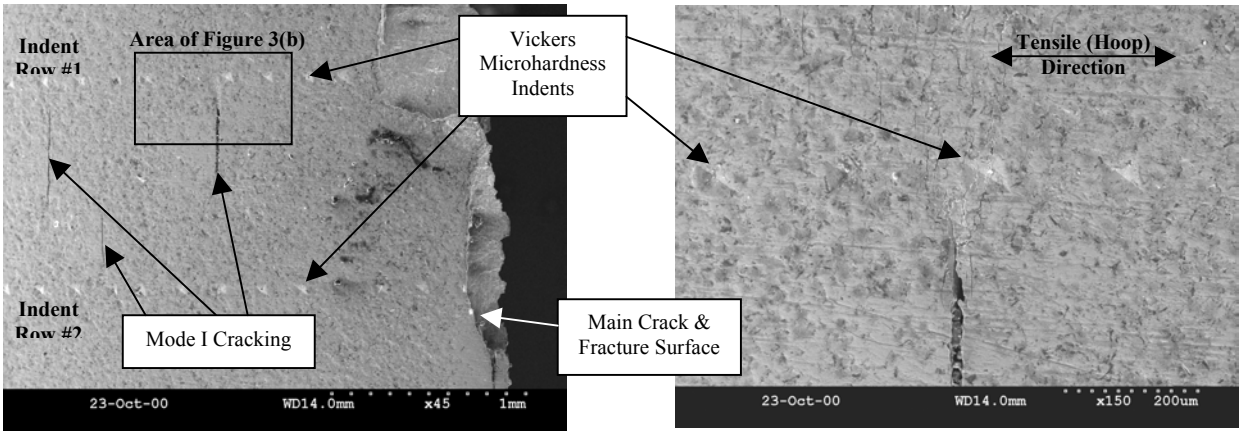

(a) (b)

FIG. 3 – Scanning electron micrographs at (a) low magnification (45X) and (b) higher magnification (150X) showing Mode I surface cracking of a plane-strain specimen (A1#2) with a hydride rim of 148 µm that was tested at room temperature.

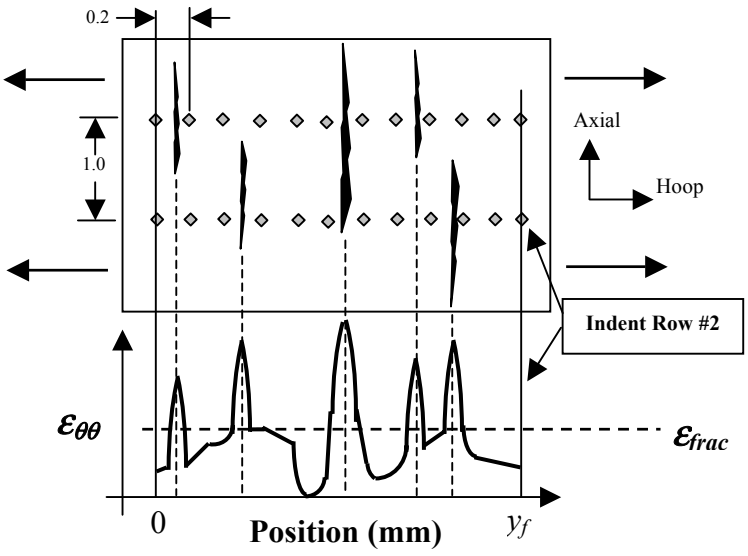

(a)

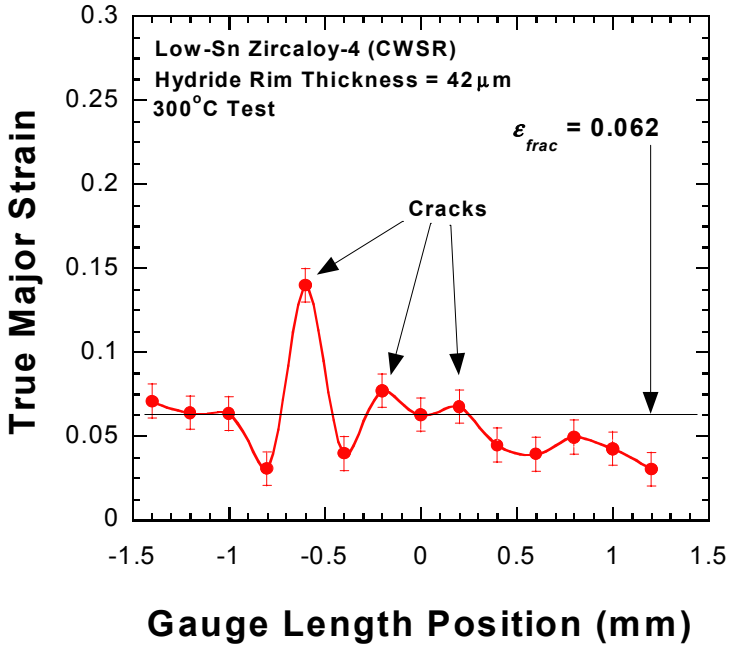

(b)

FIG. 4 – (a) Schematic of Mode I cracks with respect to microhardness indentation array and corresponding schematic of strain distribution of Indent Row #2 (dimensions in millimeters and not-to-scale) and (b) actual strain distribution of plane-strain ring-stretch specimen (N7R#1) with hydride layer thickness of 42 µm tested at 300°C.

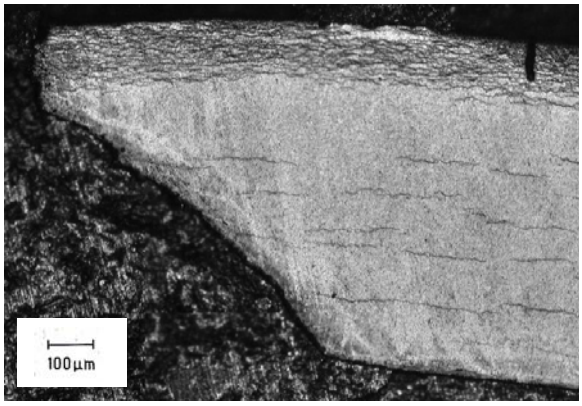

(a)

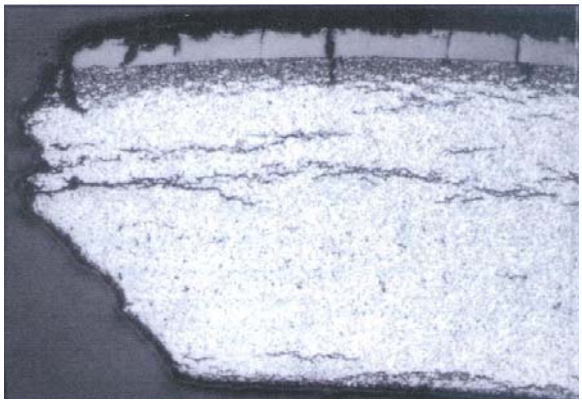

(b)

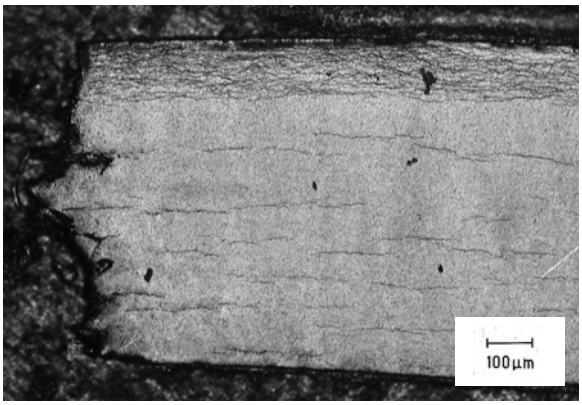

(c)

FIG. 5 – Transverse fracture profiles of Zircaloy-4 in (a) hydrided, non-irradiated condition (specimen B2#5 with a hydride rim of 101 µm that was tested at 300°C), (b) hydrided, irradiated condition [*15*] showing Mode I cracking of hydride layer followed by shear instability, and (c) hydrided, non-irradiated condition (specimen B2#2 with a hydride rim of 86 µm that was tested at room temperature) showing Mode I cracking of hydride layer followed by ductile microvoid coalescence.

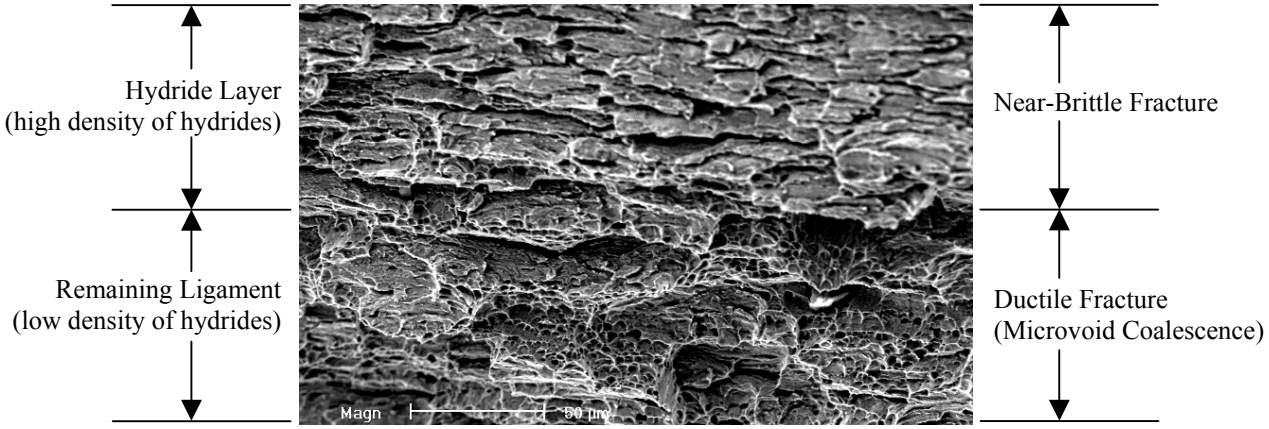

FIG. 6 – Scanning electron micrograph of fracture surface of a hydrided, non-irradiated specimen (N26#1) with a hydride rim of 245 μm that was tested at room temperature. Near-brittle fracture of hydride layer is followed by ductile microvoid coalescence within the remaining ligament.

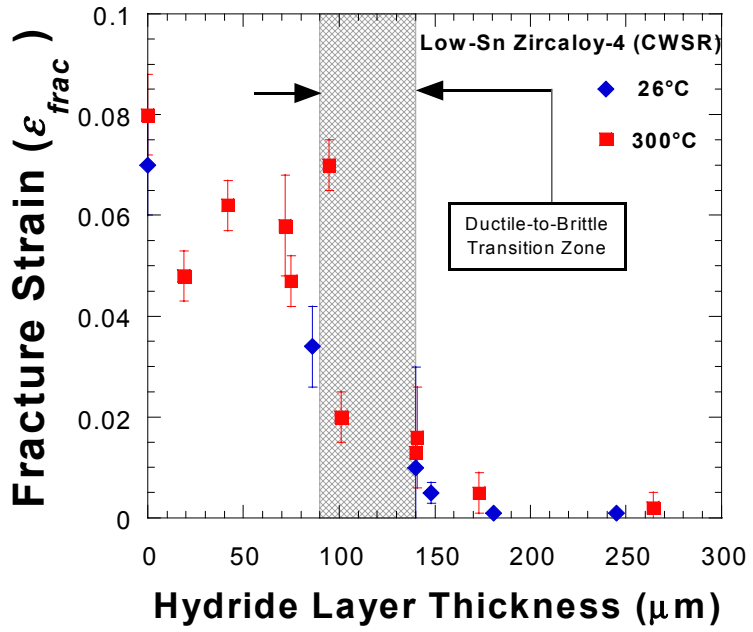

(a)

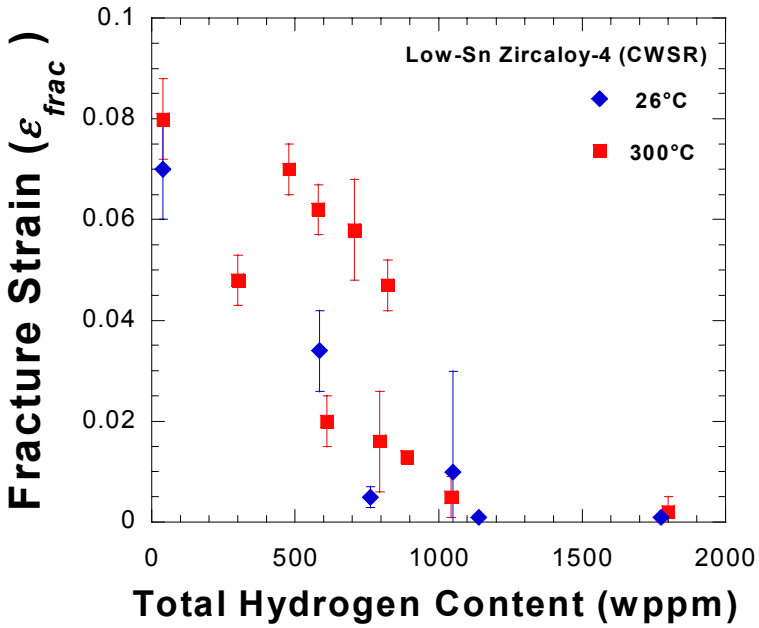

(b)

FIG. 7 –Fracture strain (ε_{frac}) at room temperature and 300°C as a function of (a) hydride layer thickness and (b) total hydrogen content.

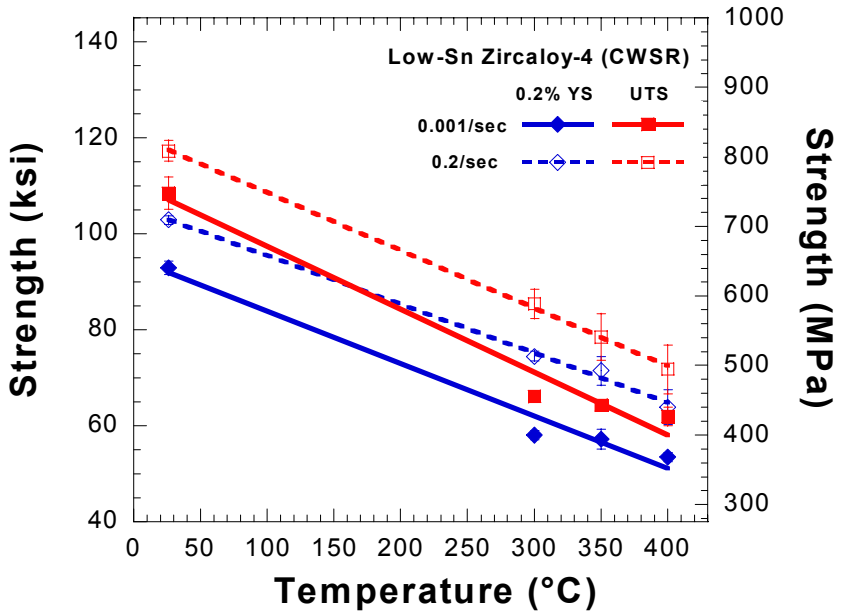

(a)

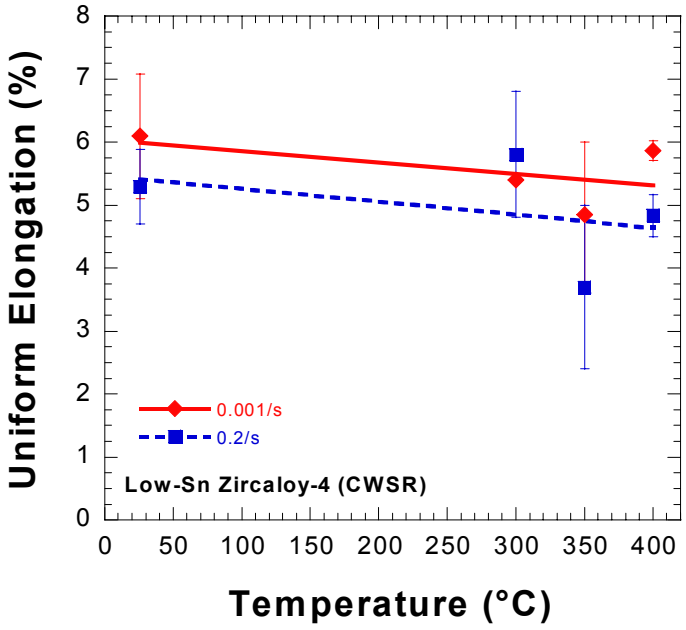

(b)

FIG. 8 – (a) Yield and ultimate tensile strengths and (b) uniform elongation for non-irradiated cladding as a function of temperature and strain rate.